Hindawi
Advances in Civil Engineering
Volume 2019, Article ID 3648650, 20 pages
https://doi.org/10.1155/2019/3648650

Research Article

Analysis of Factors Influencing Stability of Overlying Soil Layer on Thin Bedrock Based on Crack Development-Closure Test

Guangming Wu,[1] **Haibo Bai**,[1] **Luyuan Wu**,[1] **Shixin He**,[1] **and Bin Du**[1,2]

[1]*State Key Laboratory for Geomechanics and Deep Underground Engineering, China University of Mining & Technology, Xuzhou, Jiangsu 221116, China*
[2]*Jiangsu Vocational Institute of Architectural Technology, Xuzhou, Jiangsu 221116, China*

Correspondence should be addressed to Haibo Bai; hbbaiteacher@sina.com

Received 19 September 2019; Accepted 12 October 2019; Published 31 December 2019

Academic Editor: Fan Gu

The water-blocking properties of the clay layer at the bottom of the Cenozoic overburden in China are an important factor influencing the safety of thin bedrock coal seam mining. Clay has remolding properties that are unlike the nonreversible characteristics of cracks in brittle rock, and failure cracks in clay can reclose or continue to expand under the influence of different external factors. In this work, the soil layer on top of thin bedrock is the research object, and the influences of the particle composition, water content, soil layer thickness, and crack width on the crack development-closure state of soil layer are analyzed by the orthogonal test method. Visual analysis shows that the order of influence of each factor on the stability of soil layer is the crack width, particle composition, soil layer thickness, and water content. The stability of soil layer decreases with increasing crack width and sand content and decreasing soil layer thickness; in addition, soil layer stability decreases first and then increases with increasing water content. Further variance analysis shows that the crack width and particle composition are key factors that impact the stability of soil layer and that the soil layer thickness has some influence, while the water content has little effect on the stability of soil layer. In addition, the crack will reclose when the sand content in soil is less than 50% and the crack width is less than or equal to 1.0 mm, and the soil layer is prone to further failure when the sand content in soil is more than 50% and the crack width is greater than or equal to 3.0 mm; when the soil layer thickness is 15.0 cm, its stability is better than when the soil layer thickness is 10.0 cm or 5.0 cm.

1. Introduction

Environmental problems, such as water resource shortages and surface degradation caused by coal mining, are becoming increasingly prominent as the intensity of coal mining in China increases. The aforementioned is especially true in midwestern areas, where underground latent water resources are widely distributed in the Cenozoic overburden. The damage to underground latent water resources is particularly evident in the coal seam mining process [1–4]. Therefore, ideas and methods, such as "green coal mining [5–7]" and the "coexistence of coal and water [8–11]," have been proposed. These ideas and methods have provided new ways of protecting underground latent water resources.

To find solutions to specific problems, such as maintaining the safety of coal seam mining and researching the water-blocking mechanisms of clay, scholars in China and abroad have carried out useful studies by establishing safety assessment methods, conducting field measurements, and running numerical simulations. For example, the concept of the risk coefficient of water inrush in loose porous aquifers and the clay at the bottom of the Quaternary system that has been put forward can be used as part of the mining protection layer [12–15]. These studies provide guidance to improve the extent of coal seam mining under thin bedrock.

Simultaneously, much research has also been conducted on the protection of water resources in the process of mining coal resources. The influence of coal mining on underground

latent water resources were divided into four categories, namely, serious, moderate, slight, and no water loss, and an aquifer-protection mining technique can be successfully applied by modifying a few mining parameters, such as the mining height or advance rate. Moreover, the key factor in protecting underground latent water resources is the thickness of the weathered bedrock located immediately below the aquifer [16–20]. Mining activities can cause not only surface and subsurface water loss but also chemical, trace metal, and microbiological pollution of surface and subsurface water [21–25].

The water flowing fractured zone usually penetrates through thin bedrock while mining coal seams under thin bedrock. At this time, the clay layer at the bottom of the Cenozoic overburden becomes an important water-blocking structure and plays an important role in preventing the water in porous aquifers and phreatic aquifers from flowing to the working face [26]. In addition, the properties, distribution characteristics, and mining failure characteristics of clay have important influences on its water-blocking performance [27–30]. Unlike the development of dry crack or the development of crack in slopes, retaining walls, and other soil engineering structures [31–35], the direction of mining-induced shear/tension crack in the overlying soil layer during thin bedrock coal seam mining is generally nearly vertical and the crack is subject to erosion and scouring by upper phreatic aquifer water [36]. In addition, clay has remolding properties, which are unlike the nonreversible crack in brittle rock [37–40]. The crack in soil will reclose under the action of stress and water swelling property and other factors. For example, Huang et al. [41] found that the crack in the soil swelled with water and the crack reclosed when the amount of expansion exceeded the width of the crack. Zhang et al. [42, 43] studied the functional relationship between the soil suction and resilient modulus by repeated load triaxial test and considered that the resilient modulus increases with the increase in the minimum bulk stress, soil suction, and degree of compaction and decreases with increasing octahedral shear stress.

The characteristics of crack development-closure in soil layer are of great significance to the stability of the overlying soil and its water-blocking effect in thin bedrock coal seam mining. In this paper, four factors that affect the development-closure state of crack, namely, particle composition, soil layer thickness, crack width, and water content, are examined. The crack development-closure characteristics of soil layer are analyzed by the orthogonal test method. The aim of the work is to provide a reference for the stability analysis of overlying soil and the protection of underground latent water resources in thin bedrock geological regions during thin bedrock coal seam mining.

2. Hydrogeological Conditions of Thin Bedrock Coal Seam Mining

2.1. Thin Bedrock Definition. At present, there is no clear standard for the definition of thin bedrock, and researchers have different definitions of thin bedrock according to their own research purposes. For instance, thin bedrock can be defined according to the height of three zones based on the view of water prevention [44]. Similarly, researchers define thin bedrock according to whether there exists a key stratum based on the view of mine pressure control [15]. This article defines thin bedrock (as shown in Figure 1) in terms of the water prevention view [44], and (1) if the bedrock thickness H_b is smaller than the height of the caving zone H_c, it is called ultrathin bedrock; (2) if the bedrock thickness H_b is larger than the height of the caving zone H_c but smaller than the height of the water flowing fractured zone $H_c + H_f$, it is called thin bedrock; and moreover, (3) if the bedrock thickness H_b is larger than the height of the water flowing fractured zone $H_c + H_f$, it is called normal thickness bedrock. Ultrathin bedrock and thin bedrock are commonly referred to as thin bedrock.

2.2. Hydrogeological Conditions of Thin Bedrock. The Carboniferous and Permian (C_3-P_1) and Jurassic (J_1-J_2) are the main coal forming periods in China (as shown in Figure 2). Tectonism leads to interruption or denudation in the strata deposit after the deposition of coal measure strata has been completed. As a result, some of the strata between the coal measure strata and the Cenozoic overburden are missing, and the Cenozoic overburden is directly deposited on the coal measure strata (as shown in Figure 3).

The water flowing fractured zone generally penetrates through thin bedrock and into the Cenozoic overburden with the progression of coal mining under such geological conditions. Accordingly, the failure state and water-blocking properties of soil in the Cenozoic overburden are key factors in determining whether a hydraulic connection between the Cenozoic porous aquifers and the working face will occur. Typical hydrogeological conditions of thin bedrock are shown in Figure 3.

2.3. Failure Process of the Overlying Soil of Thin Bedrock. The overlying soil layer of thin bedrock will deform or even fail with the deformation and caving of the bedrock as the coal seam is continuously exploited, and the process of deformation and failure of the overlying soil layer can be divided into three stages, as shown in Figure 4. First, the coal seam is mined out. Second, the bedrock collapses or fractures. Third, the collapse or fracture of the thin bedrock leads to a reduction in the supporting space of the overlying soil layers, and the overlying soil layers will subside due to the self-weight load. Then, the overlying soil layers undergo deformation and failure. Consequently, the essential cause of deformation or failure of the soil is the reduction in the supporting space in its lower part.

The overlying soil will deform and produce cracks under the influence of coal seam mining. The cracks may reclose or continue to broaden by scouring and finally lead to further soil destruction under the action of water flow scouring in loose porous aquifer and other conditions. The key factors affecting the development-closure state of the cracks in soil layer are particle composition, dry-wet state (which can be expressed by the saturation or water content), crack dimension (crack length and width), and soil stress state.

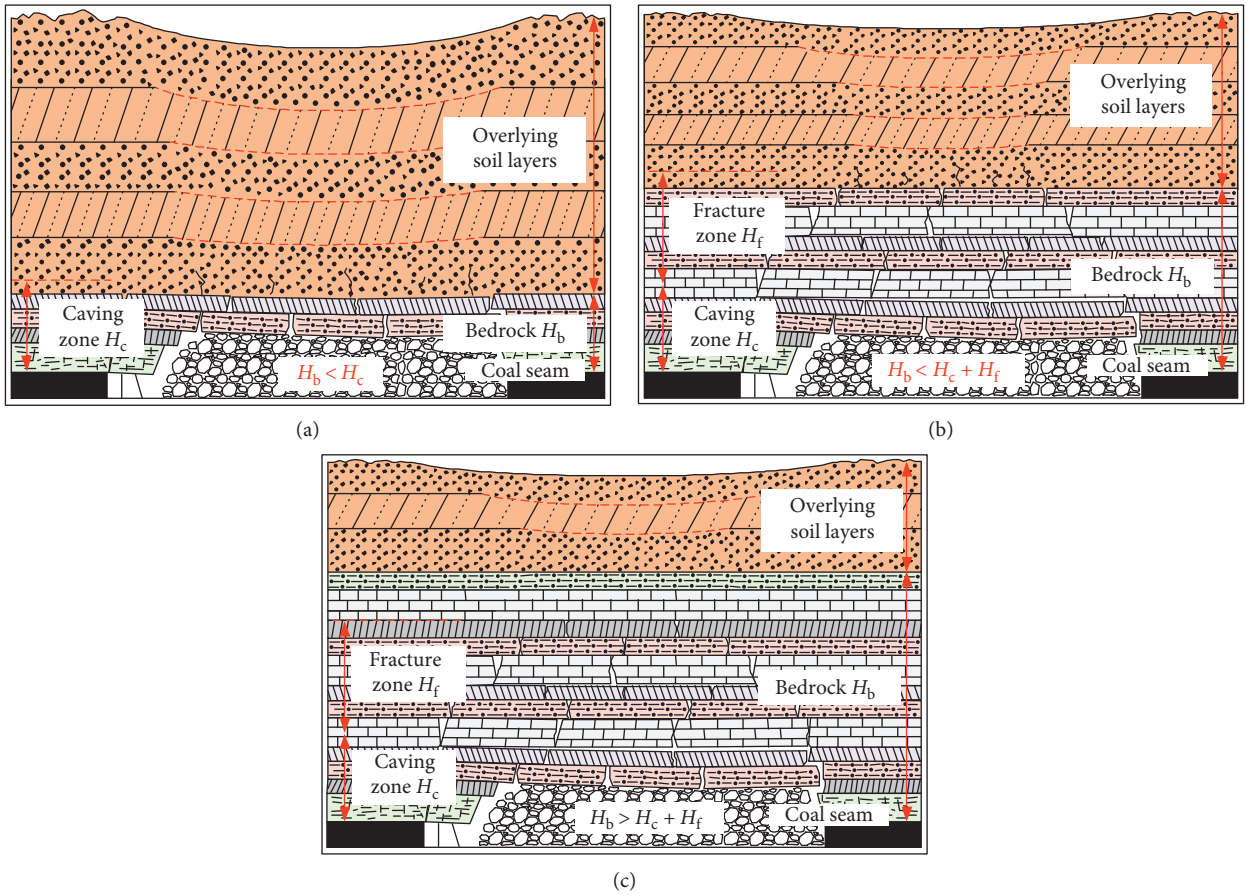

Figure 1: Classification diagram of bedrock: (a) ultrathin bedrock, $H_b < H_c$; (b) thin bedrock, $H_b < H_c + H_f$; (c) normal thickness bedrock, $H_b > H_c + H_f$.

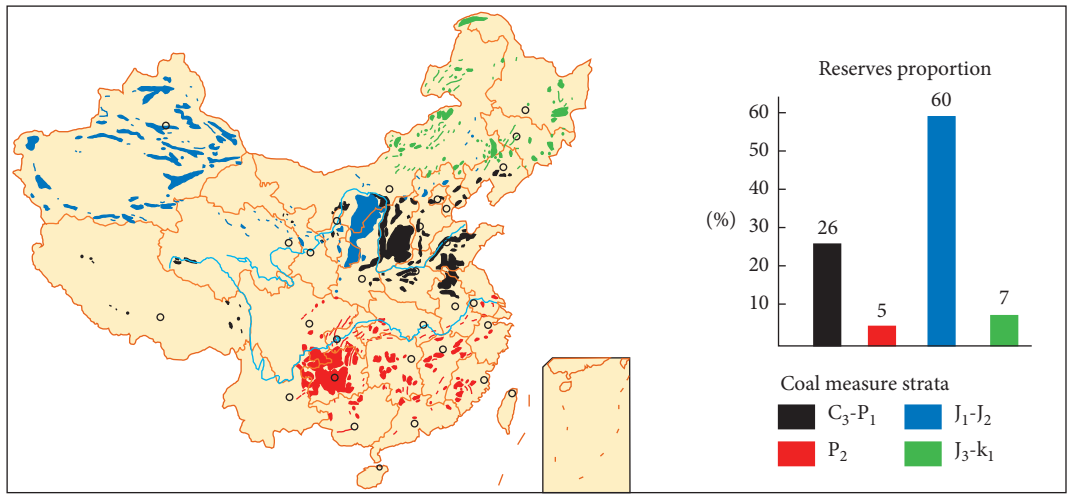

Figure 2: Distribution diagram of the major coal resources in China.

The main external forces are the self-weight stress and phreatic aquifer hydrostatic pressure in the overlying soil of thin bedrock, and their influence mode is long-term slow action. Therefore, the influence of the dynamic change in external forces can be temporarily neglected. Then, four factors can be selected, namely, the soil particle composition, water content, crack length, and crack width, and influence analysis of these factors on the development-closure state of the cracks in soil layer can be performed through orthogonal experimental methods.

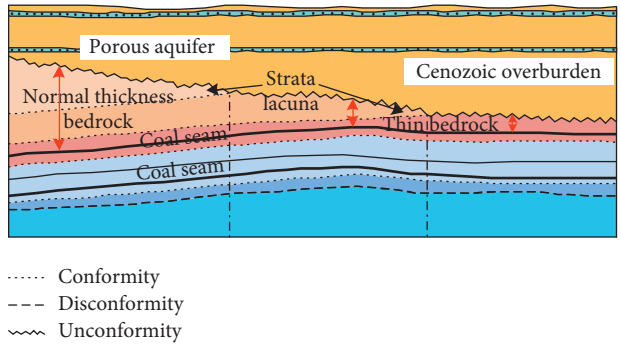

Figure 3: Hydrogeological profile of thin bedrock.

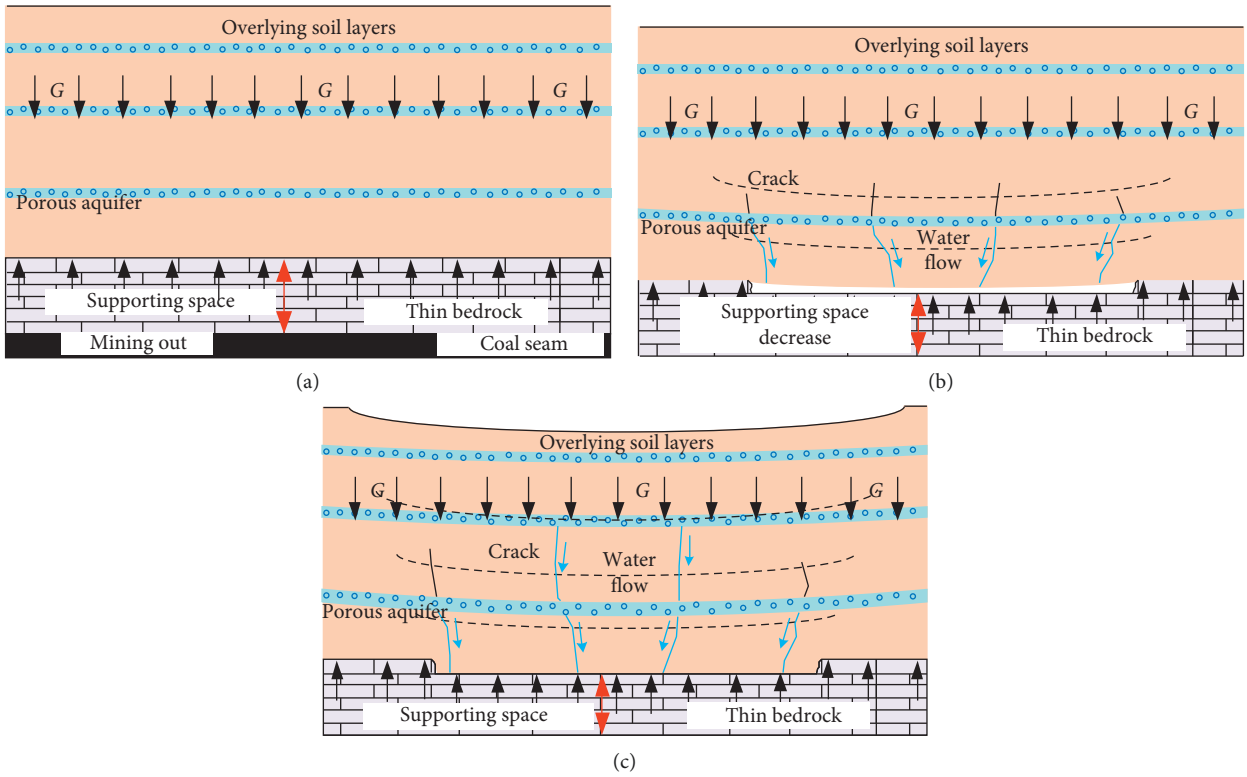

Figure 4: Failure process of the overlying soil layers of thin bedrock: (a) natural state; (b) coal seam mining out ⟹ thin bedrock collapses or fractures ⟹ supporting space decreases and soil layer subside; (c) overlying soil layers recompact on the collapsed thin bedrock.

3. Experimental Device and Scheme

3.1. Experimental Device and Specimen Preparation. The crack development-closure experimental device for soil layer is shown in Figure 5.

The main functions of the experimental device are as follows: (1) the water tanks I and II, the water inlet pipe, and the overflow pipe keep the water level above the soil layer constant; that is, a constant hydrostatic pressure is maintained and (2) the volume of outflow water from the cracks is measured by using a measuring cylinder, and the flow volume can be calculated in terms of the volume of outflow water.

The change in soil particle composition is simulated by changing the ratio of bentonite clay to fine sand (0.075 mm < particle diameter ≤ 0.25 mm), which is shown in Figure 6. The higher the sand content is, the lower the content of hydrophilic minerals in the soil is, and the worse the hydrophilicity and water swelling properties of the soil are.

The water content is realized by adding water. First, the dry weight of the soil layer is calculated in terms of the soil density (1.884 g/cm^3). Then, the quality of water needed to added can be calculated according to the water content. The crack length means the length of the crack in the vertical direction, and the cracks in the soil layer are actually not straight. The cracks made in experiments are straight cracks because it is difficult to make bending cracks in specimens; therefore, the thickness of the soil layer is equal to the crack

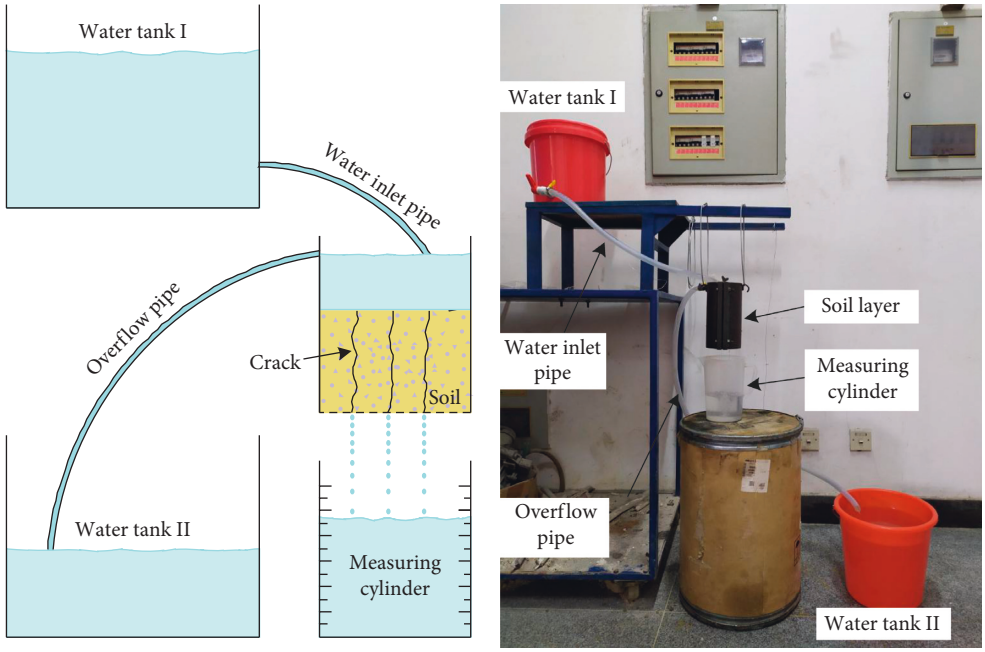

(a) (b)

Figure 5: Experimental device for crack development-closure in soil layer: (a) schematic diagram of the experimental device; (b) experimental device.

(a) (b)

Figure 6: Soil composition: (a) bentonite clay; (b) fine sand.

length. A crack is formed when the iron wire penetrates the soil layer after the soil layer was compacted and formed according to the design thickness (as shown in Figure 7).

3.2. Experimental Scheme. The symbols of each factor in the experiments and their level values are shown in Table 1.

There are four factors in the experiments, and each factor has three levels. The purpose of the experiments is to analyze the influence of four factors on the development-closure state of the cracks in soil layer. Simultaneously, the effect of the interaction between the particle composition and the other factors on the crack development-closure state is emphatically investigated. The free degree of four experimental factors (each of which has three levels) and four sets of interactions is $4 \times (3-1) + 4 \times (3-1) \times (3-1) = 24$; therefore, the $L_{27}(3^{13})$ orthogonal table can be used to design the experimental scheme, which is shown in Table 2.

The dependent variable of the experiments is the development-closure state of the cracks in soil layer, that is, the change in crack dimension, and the water rate of flow Q can be used to indicate the change in soil crack dimension (the water rate of flow is defined as the volume of fluid flow through cracks per unit time, and the unit is m^3/s). Then, the development-closure state of the cracks in soil layer can be determined according to the change trend of Q. (1) The water rate of flow Q decreases gradually to $0\,m^3/s$, which indicates that the crack dimension gradually decreases to closure. (2) The water rate of flow Q gradually increases to $\infty\,m^3/s$, which means that the crack gradually broadens due to water flow scouring and finally leads to soil further destruction. (3) The water rate of flow Q is between $0\,m^3/s$ and

(a) (b) (c)

Figure 7: Production drawing of cracks in soil: (a) iron wires of different diameters; (b) crack fabrication process; (c) crack formation.

Table 1: Experimental factors and their level values.

Level	Factor Symbol	Particle composition Cc	Water content ω	Soil layer thickness Cl	Crack width Cw
1		Cc_{10} (soil-sand ratio 1 : 0)	ω_{15} (15%)		Cw_1 (1.0 mm)
2		Cc_{11} (soil-sand ratio 1 : 1)	ω_{20} (20%)	Cl_{10} (10.0 cm)	Cw_2 (2.0 mm)
3		Cc_{13} (soil-sand ratio 1 : 3)	ω_{25} (25%)	Cl_{15} (15.0 cm)	Cw_3 (3.0 mm)

∞ m^3/s, which indicates that the crack is ultimately neither reclosed nor broadened by water flow scouring.

4. Experimental Results and Discussion

4.1. Direct Analysis of the Experimental Results

4.1.1. Experimental Results. The water rate of flow results at 6 h for each experiment is shown in Table 3.

Table 3 shows that the water rate of flow for 6 of the 27 experiments (experiments 1, 4, 7, 10, 13, and 16) gradually decreases to 0 m^3/s, which indicates that the cracks in the soil finally reclose under the experimental conditions of these 6 experiments. There are 19 experiments (experiments 2, 3, 5, 6, 8, 9, 11, 12, 14, 15, 17, 18, 19, 20, 22, 23, 25, 26, and 27) whose water rate of flow is between 0 m^3/s and ∞ m^3/s, which indicates that the cracks are ultimately neither reclosed nor broadened by water flow scouring under these 19 experimental conditions. The water rate of flow for 2 of the 27 experiments (experiments 21 and 24) gradually increases to ∞ m^3/s, which indicates that the cracks gradually broaden due to water flow scouring and finally lead to soil destruction under the experimental conditions of these 2 experiments.

4.1.2. Analysis of Experiments That the Water Rate of Flow Decreases Gradually to 0 m^3/s. One comparison of the initial cracks and reclosed cracks in the experiments in which the water rate of flow decreases gradually to 0 m^3/s is shown in Figure 8.

The water rate of flow curves changes with time in the experiments in which the water rate of flow gradually decreases to 0 m^3/s is shown in Figure 9.

As shown in Figure 9, the water rate of flow of the 6 groups gradually decreases to 0 m^3/s (that is, the cracks reclosed in these experiments) under the same experimental conditions of $Cc_{10} \cap Cw_1$ or $Cc_{11} \cap Cw_1$, which indicates that when the ratio of soil to sand is greater than or equal to 1 : 1 and the crack width is less than or equal to 1.0 mm, the cracks are reclosed regardless of the thickness and water content of the soil. At the same time, the period with a sharp decrease in the water rate of flow in the 6 experiments is less than 20 minutes, which shows that the duration of the main change in the soil swelling increment Δs (or water swelling velocity rate $v_s(t)$) and soil compaction amount Δc (or compression velocity rate $v_c(t)$) is less than 20 minutes, namely, the sum of the swelling increment Δs and compaction amount Δc is larger than the sum of the broadening amount Δb and original crack width Cw_o, which results in the cracks reclosed.

4.1.3. Analysis of Experiments That the Water Rate of Flow between 0 m^3/s and ∞ m^3/s. A comparison of the initial and stable cracks in the experiments in which the water rate of flow is between 0 m^3/s and ∞ m^3/s is shown in Figure 10.

The water rate of flow curves changes with time in the experiments in which the water rate of flow is between 0 m^3/s and ∞ m^3/s is shown in Figure 11.

As shown in Figure 11, the water rate of flow of experiment 27 is the largest and is 12.167 (10^{-6} m^3/s), while that of experiment 25 is the smallest and is 0.008 (10^{-6} m^3/s). Intuitively, it cannot be determined which factor is the main factor and which factor is the secondary factor leading to the difference in the rate of flow results. Thus, further analysis of the experimental results is needed to determine the order of influence of each experimental factor on the water rate of flow.

4.1.4. Analysis of Experiments That the Soil Layer Destroyed. One comparison of the initial cracks and destroyed soil in the experiments in which the water rate of flow increases gradually to ∞ m^3/s is shown in Figure 12.

Table 2: Experimental schemes for the crack development-closure state of soil layer.

Experiment number	Column Factor	1 Cc	2 Cl	3	4 Cc × Cl	5 Cw	6	7 Cc × Cw	8	9 Cl × Cw	10 ω	11	12 Cc × C_ω	13	Scheme number
1		1	1	1	1	1	1	1	1	1	1	1	1	1	Cc_{10} Cl_5 Cw_1 ω_{15}
2		1	1	1	1	2	2	2	2	2	2	2	2	2	Cc_{10} Cl_5 Cw_2 ω_{20}
3		1	1	1	1	3	3	3	3	3	3	3	3	3	Cc_{10} Cl_5 Cw_3 ω_{25}
4		1	2	2	2	1	1	1	2	2	2	3	3	3	Cc_{10} Cl_{10} Cw_1 ω_{20}
5		1	2	2	2	2	2	2	3	3	3	1	1	1	Cc_{10} Cl_{10} Cw_2 ω_{25}
6		1	2	2	2	3	3	3	1	1	1	2	2	2	Cc_{10} Cl_{10} Cw_3 ω_{15}
7		1	3	3	3	1	1	1	3	3	3	2	2	2	Cc_{10} Cl_{15} Cw_1 ω_{25}
8		1	3	3	3	2	2	2	1	1	1	3	3	3	Cc_{10} Cl_{15} Cw_2 ω_{15}
9		1	3	3	3	3	3	3	2	2	2	1	1	1	Cc_{10} Cl_{15} Cw_3 ω_{20}
10		2	1	2	3	1	2	3	1	2	3	1	2	3	Cc_{11} Cl_5 Cw_1 ω_{25}
11		2	1	2	3	2	3	1	2	3	1	2	3	1	Cc_{11} Cl_5 Cw_2 ω_{15}
12		2	1	2	3	3	1	2	3	1	2	3	1	2	Cc_{11} Cl_5 Cw_3 ω_{20}
13		2	2	3	1	1	2	3	2	3	1	3	1	2	Cc_{11} Cl_{10} Cw_1 ω_{15}
14		2	2	3	1	2	3	1	3	1	2	1	2	3	Cc_{11} Cl_{10} Cw_2 ω_{20}
15		2	2	3	1	3	1	2	1	2	3	2	3	1	Cc_{11} Cl_{10} Cw_3 ω_{25}
16		2	3	1	2	1	2	3	3	1	2	2	3	1	Cc_{11} Cl_{15} Cw_1 ω_{20}
17		2	3	1	2	2	3	1	1	2	3	3	1	2	Cc_{11} Cl_{15} Cw_2 ω_{25}
18		2	3	1	2	3	1	2	2	3	1	1	2	3	Cc_{11} Cl_{15} Cw_3 ω_{15}
19		3	1	3	2	1	3	2	1	3	2	1	3	2	Cc_{13} Cl_5 Cw_1 ω_{20}
20		3	1	3	2	2	1	3	2	1	3	2	1	3	Cc_{13} Cl_5 Cw_2 ω_{25}
21		3	1	3	2	3	2	1	3	2	1	3	2	1	Cc_{13} Cl_5 Cw_3 ω_{15}
22		3	2	1	3	1	3	2	2	1	3	3	2	1	Cc_{13} Cl_{10} Cw_1 ω_{25}
23		3	2	1	3	2	1	3	3	2	1	1	3	2	Cc_{13} Cl_{10} Cw_2 ω_{15}
24		3	2	1	3	3	2	1	1	3	2	2	1	3	Cc_{13} Cl_{10} Cw_3 ω_{20}
25		3	3	2	1	1	3	2	3	2	1	2	1	3	Cc_{13} Cl_{15} Cw_1 ω_{15}
26		3	3	2	1	2	1	3	1	3	2	3	2	1	Cc_{13} Cl_{15} Cw_2 ω_{20}
27		3	3	2	1	3	2	1	2	1	3	1	3	2	Cc_{13} Cl_{15} Cw_3 ω_{25}

Table 3: Experimental results of crack development-closure in soil layer.

Experiment number	Column	1	2	3	4	5	6	7	8	9	10	11	12	13	Experimental results: Q_i (10^{-6} m^3/s)
	Factor	Cc	Cl	Cc × Cl		Cw	Cc × Cw		Cl × Cw		ω	Cc × ω			
1		1	1	1	1	1	1	1	1	1	1	1	1	1	0.000
2		1	1	1	1	2	2	2	2	2	2	2	2	2	1.517
3		1	1	1	1	3	3	3	3	3	3	3	3	3	9.758
4		1	2	2	2	1	1	1	2	2	2	3	3	3	0.000
5		1	2	2	2	2	2	2	3	3	3	1	1	1	1.442
6		1	2	2	2	3	3	3	1	1	1	2	2	2	3.667
7		1	3	3	3	1	1	1	3	3	3	2	2	2	0.000
8		1	3	3	3	2	2	2	1	1	1	3	3	3	0.650
9		1	3	3	3	3	3	3	2	2	2	1	1	1	5.375
10		2	1	2	3	1	2	3	1	2	3	1	2	3	0.000
11		2	1	2	3	2	3	1	2	3	1	2	3	1	2.433
12		2	1	2	3	3	1	2	3	1	2	3	1	2	11.183
13		2	2	3	1	1	2	3	2	3	1	3	1	2	0.000
14		2	2	3	1	2	3	1	3	1	2	1	2	3	2.050
15		2	2	3	1	3	1	2	1	2	3	2	3	1	10.325
16		2	3	1	2	1	2	3	3	1	2	2	3	1	0.000
17		2	3	1	2	2	3	1	1	2	3	3	1	2	1.800
18		2	3	1	2	3	1	2	2	3	1	1	2	3	6.033
19		3	1	3	2	1	3	2	1	3	2	1	3	2	0.483
20		3	1	3	2	2	1	3	2	1	3	2	1	3	6.508
21		3	1	3	2	3	2	1	3	2	1	3	2	1	∞
22		3	2	1	3	1	3	2	2	1	3	3	2	1	0.783
23		3	2	1	3	2	1	3	3	2	1	1	3	2	4.583
24		3	2	1	3	3	2	1	1	3	2	2	1	3	∞
25		3	3	2	1	1	3	2	3	2	1	2	1	3	0.008
26		3	3	2	1	2	1	3	1	3	2	3	2	1	0.975
27		3	3	2	1	3	2	1	2	1	3	1	3	2	12.167

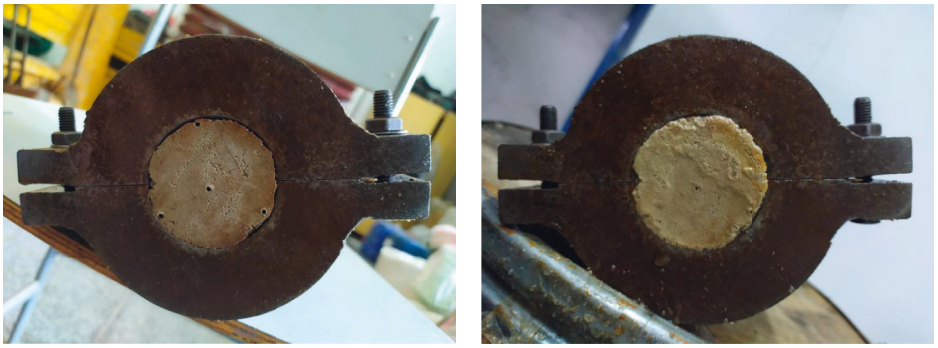

(a) (b)

Figure 8: One comparison of the initial cracks and reclosed cracks: (a) initial cracks of experiment No. 10; (b) cracks reclosed of experiment No. 10.

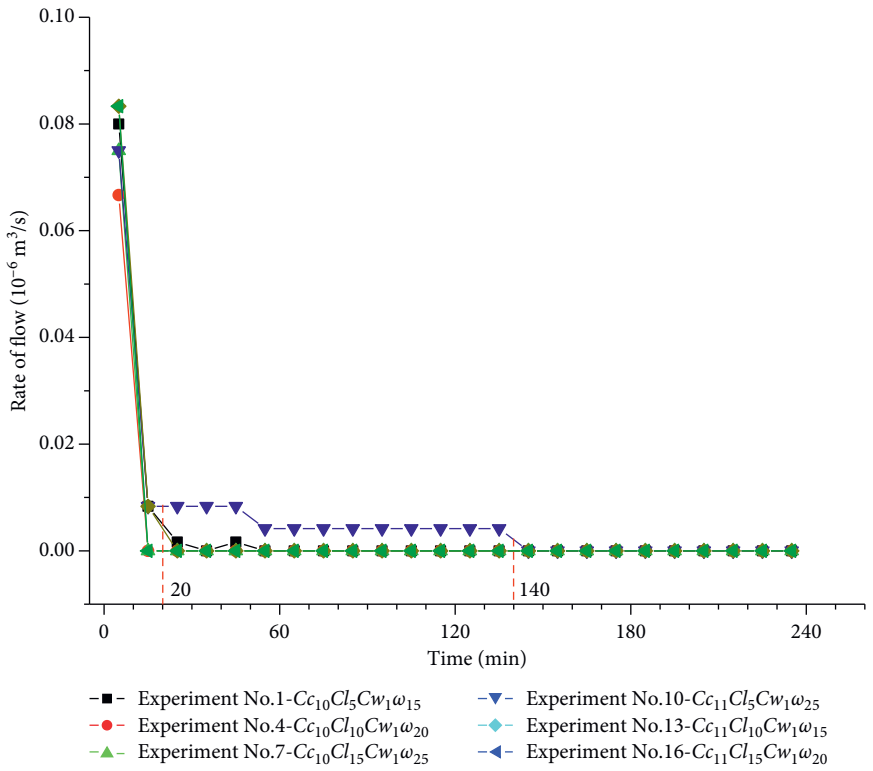

Figure 9: Change curve of the crack rate of flow that decreases to 0 m^3/s.

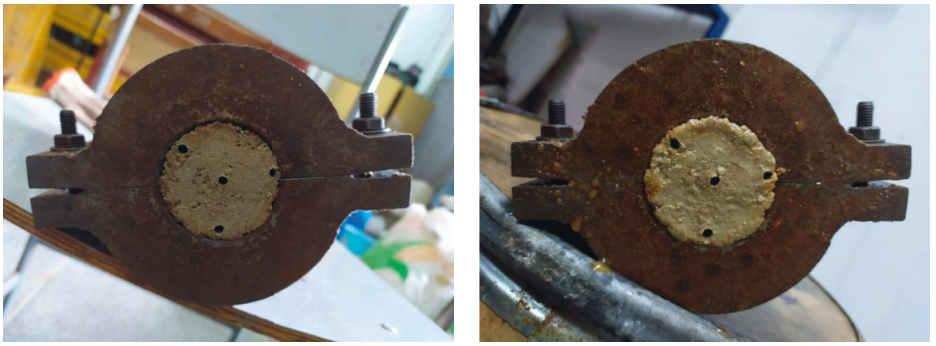

(a) (b)

Figure 10: One comparison of the initial cracks and stable cracks: (a) initial cracks of experiment No. 12; (b) cracks steady of experiment No. 12.

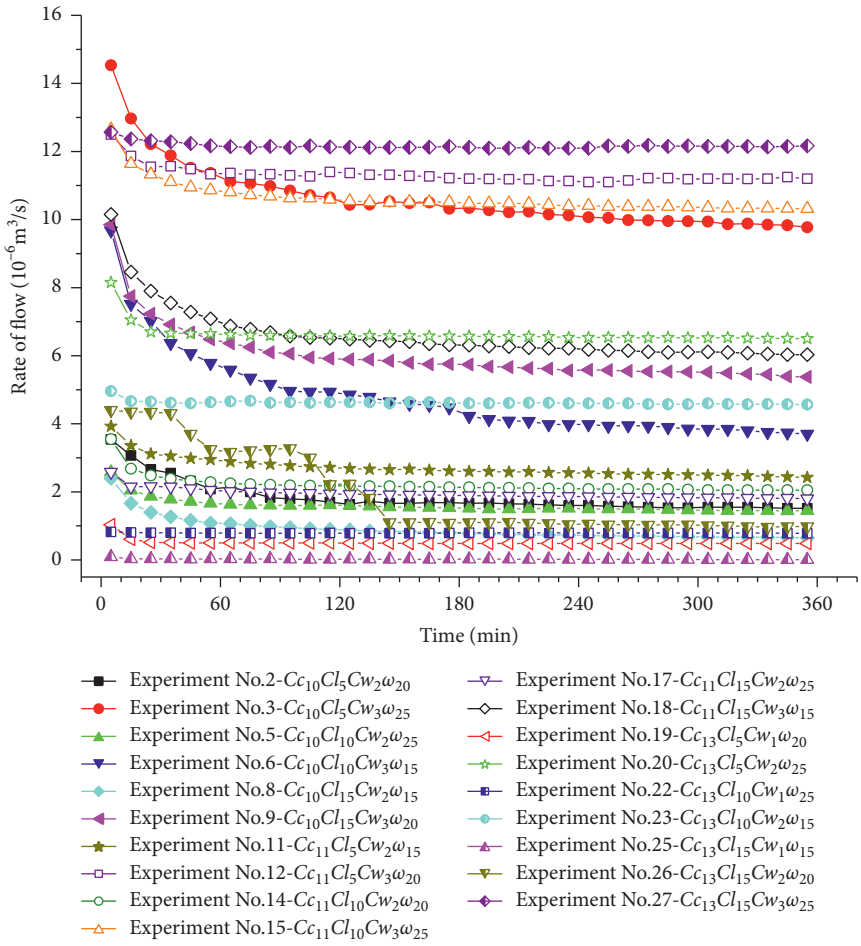

Figure 11: Change curve of the crack rate of flow between 0 m^3/s and ∞ m^3/s.

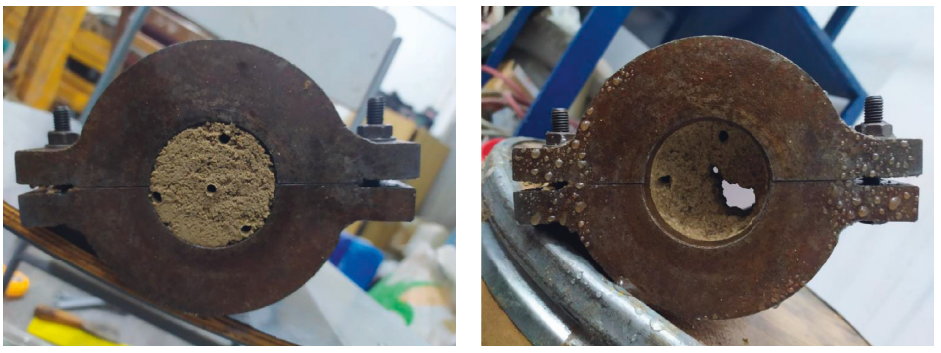

(a) (b)

Figure 12: One comparison of the initial cracks and destroyed soil layer: (a) initial cracks of experiment No. 21; (b) cracks broaden lead to soil destruction of experiment No. 21.

The water rate of flow curves changes with time in the experiments in which the water rate of flow increases to ∞ m^3/s is shown in Figure 13.

As shown in Figure 13, the condition for cracks to be broadened by scouring causing further soil destruction is $Cc_{13} \cap Cw_3$, and experiment 21 shows that the time from broadening of the crack by scouring to soil destruction is 25 minutes, while that in experiment 24, it is 310 minutes, which indicates that increasing the soil layer thickness or increasing the water content or both together can effectively increase the antidestructive capacity of the soil layer. Further analysis is needed to determine which conditions change to improve the antidestructive capacity of soil layer.

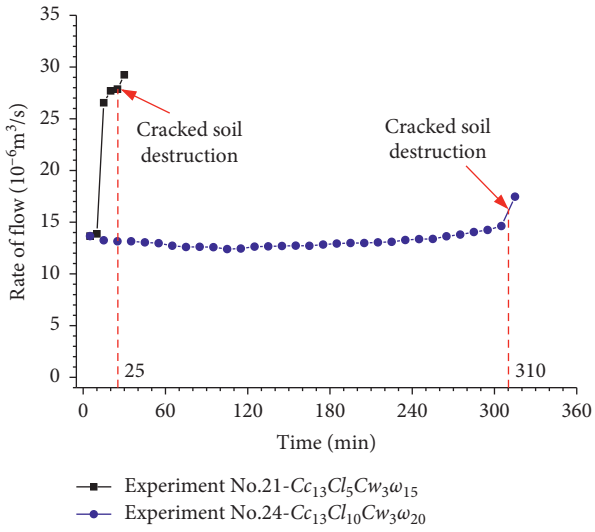

FIGURE 13: Change curve of the crack rate of flow that increases to ∞ m^3/s.

4.1.5. Analysis of Experimental Results. The experimental results show that the crack will close when the sand content in soil is less than 50% and the crack width is less than or equal to 1.0 mm and the soil layer is prone to further failure when the sand content in soil is more than 50% and the crack width is greater than or equal to 3.0 mm. The experimental results preliminarily reveal that the greater the sand content and the wider the crack width and the smaller the thickness of the soil layer, the worse the stability of the soil layer, because the orthogonal test method is adopted instead of the comprehensive test method, and visual analysis and variance analysis are needed to get more accurate conclusions.

4.2. Visual Analysis of the Experimental Results. There are 27 groups of experimental results in Table 3, and no two experiments among the 27 groups have identical experimental conditions; thus, it is not feasible to compare any of the 27 groups of experimental results directly. However, if these 27 sets of experimental results are combined, comparability of the orthogonal test results will be achieved.

Taking Cc as an example and level 1 (Cc_{10}) of experimental factor Cc appeared in experiment Nos. 1–9 in Table 3, the average of the rate of flow of these nine experiments is

$$\begin{aligned}\overline{Q_{Cc_{10}}} &= \frac{1}{9}\left(Q_1 + Q_2 + Q_3 + Q_4 + Q_5 + Q_6 + Q_7 + Q_8 + Q_9\right)\\ &= \frac{1}{9}\left(0 + 1.517 + 9.758 + 0 + 1.442 + 3.667 + 0 + 0.650 + 5.375\right)\\ &= 2.490\left(10^{-6}\ \mathrm{m}^3/\mathrm{s}\right),\end{aligned} \tag{1}$$

level 2 (Cc_{11}) of experimental factor Cc appeared in experiment Nos. 10–18 in Table 3, the average of the rate of flow of these nine experiments is

$$\begin{aligned}\overline{Q_{Cc_{11}}} &= \frac{1}{9}\left(Q_{10} + Q_{11} + Q_{12} + Q_{13} + Q_{14} + Q_{15} + Q_{16} + Q_{17} + Q_{18}\right)\\ &= \frac{1}{9}\left(0 + 2.433 + 11.183 + 0 + 2.050 + 10.325 + 0 + 1.800 + 6.033\right)\\ &= 3.758\left(10^{-6}\ \mathrm{m}^3/\mathrm{s}\right),\end{aligned} \tag{2}$$

and level 3 (Cc_{13}) of experimental factor Cc appeared in experiment Nos. 19–27 in Table 3, the average of the rate of flow of these nine experiments is

$$\begin{aligned}\overline{Q_{Cc_{13}}} &= \frac{1}{9}\left(Q_{19} + Q_{20} + Q_{21} + Q_{22} + Q_{23} + Q_{24} + Q_{25} + Q_{26} + Q_{27}\right)\\ &= \frac{1}{9}\left(0.483 + 6.508 + 100 + 0.783 + 4.583 + 100 + 0.008 + 0.975 + 12.167\right)\\ &= 25.056\left(10^{-6}\ \mathrm{m}^3/\mathrm{s}\right).\end{aligned} \tag{3}$$

The soil layer in experiment No. 21 and No. 24 is destroyed, and their experimental results are ∞ m^3/s. Because the value ∞ cannot participate in the calculation, the rate of flow result in experiment No. 21 and No. 24 is calculated to be a larger value of 100 (10^{-6} m^3/s).

$\overline{Q_{Cc_{10}}} < \overline{Q_{Cc_{11}}} < \overline{Q_{Cc_{13}}}$, namely, the rate of flow is the largest when the particle composition is Cc_{13}, and the rate of flow is the smallest when the particle composition is Cc_{10}. This shows that the soil layer is prone to further failure when the particle composition is Cc_{13}, and the soil layer is prone to maintain stability when the particle composition is Cc_{10}.

The above calculations can also be performed in the orthogonal table, as shown in Table 4. I_j represents the sum of the experimental rate of flow results corresponding to level 1 of column j, and $\overline{I_j}$ is the average of I_j; II_j represents the sum of the experimental rate of flow results corresponding to level 2 of column j, and $\overline{II_j}$ is the average of II_j; III_j represents the sum of the experimental rate of flow results corresponding to level 3 of column j, and $\overline{III_j}$ is the average of III_j.

The experimental factor Cc is in the first column; therefore, $\overline{I_1}$ is $\overline{Q_{Cc_{10}}}$, $\overline{II_1}$ is $\overline{Q_{Cc_{11}}}$, and $\overline{III_1}$ is $\overline{Q_{Cc_{13}}}$. Similarly, Cl, Cw, and ω are in the second, fifth, and tenth columns, respectively. Hence, $\overline{I_2}$ is $\overline{Q_{Cl_5}}$, $\overline{II_2}$ is $\overline{Q_{Cl_{10}}}$, and $\overline{III_2}$ is $\overline{Q_{Cl_{15}}}$, while $\overline{I_5}$ is $\overline{Q_{Cw_1}}$, $\overline{II_5}$ is $\overline{Q_{Cw_2}}$, and $\overline{III_5}$ is $\overline{Q_{Cw_3}}$; in addition, $\overline{I_{10}}$ is $\overline{Q_{\omega_{15}}}$, $\overline{II_{10}}$ is $\overline{Q_{\omega_{20}}}$, and $\overline{III_{10}}$ is $\overline{Q_{\omega_{25}}}$.

The $\overline{I}$, $\overline{II}$, and $\overline{III}$ values of each experimental factor in Table 4 are plotted using the longitudinal coordinate system, as shown in Figure 14.

It is easy to intuitively observe that if one experimental factor has a great influence on the experimental result, then

Table 4: Visual analysis of the experimental results of crack development-closure in soil layer.

Experiment number	Column Factor	1 Cc	2 Cl	5 Cw	10 ω	Experimental results: Q_i (10^{-6} m^3/s)
1		1	1	1	1	0.000
2		1	1	2	2	1.517
⋮	⋮	⋮	⋮	⋮	⋮	⋮
26		3	3	2	2	0.975
27		3	3	3	3	12.167
I_j		22.409	131.882	1.274	117.374	
II_j		33.824	122.850	21.958	121.583	
III_j		225.507	27.008	258.508	42.783	
$\overline{I_j} = I_j/9$		2.490	14.654	0.142	13.042	
$\overline{II_j} = II_j/9$		3.758	13.650	2.440	13.509	
$\overline{III_j} = III_j/9$		25.056	3.001	28.723	4.754	
$\overline{I_j} - \overline{II_j}$		−1.268	1.004	−2.298	−0.467	
$\overline{I_j} - \overline{III_j}$		−22.566	11.653	−28.581	8.288	
$\overline{II_j} - \overline{III_j}$		−21.298	10.649	−26.283	8.755	

The soil layer in experiment No. 21 and No. 24 is destroyed, and their experimental results tend to ∞ m^3/s. Because the value ∞ cannot participate in the calculation, the rate of flow result in experiment No. 21 and No. 24 is calculated to be a larger value of 100 (10^{-6} m^3/s).

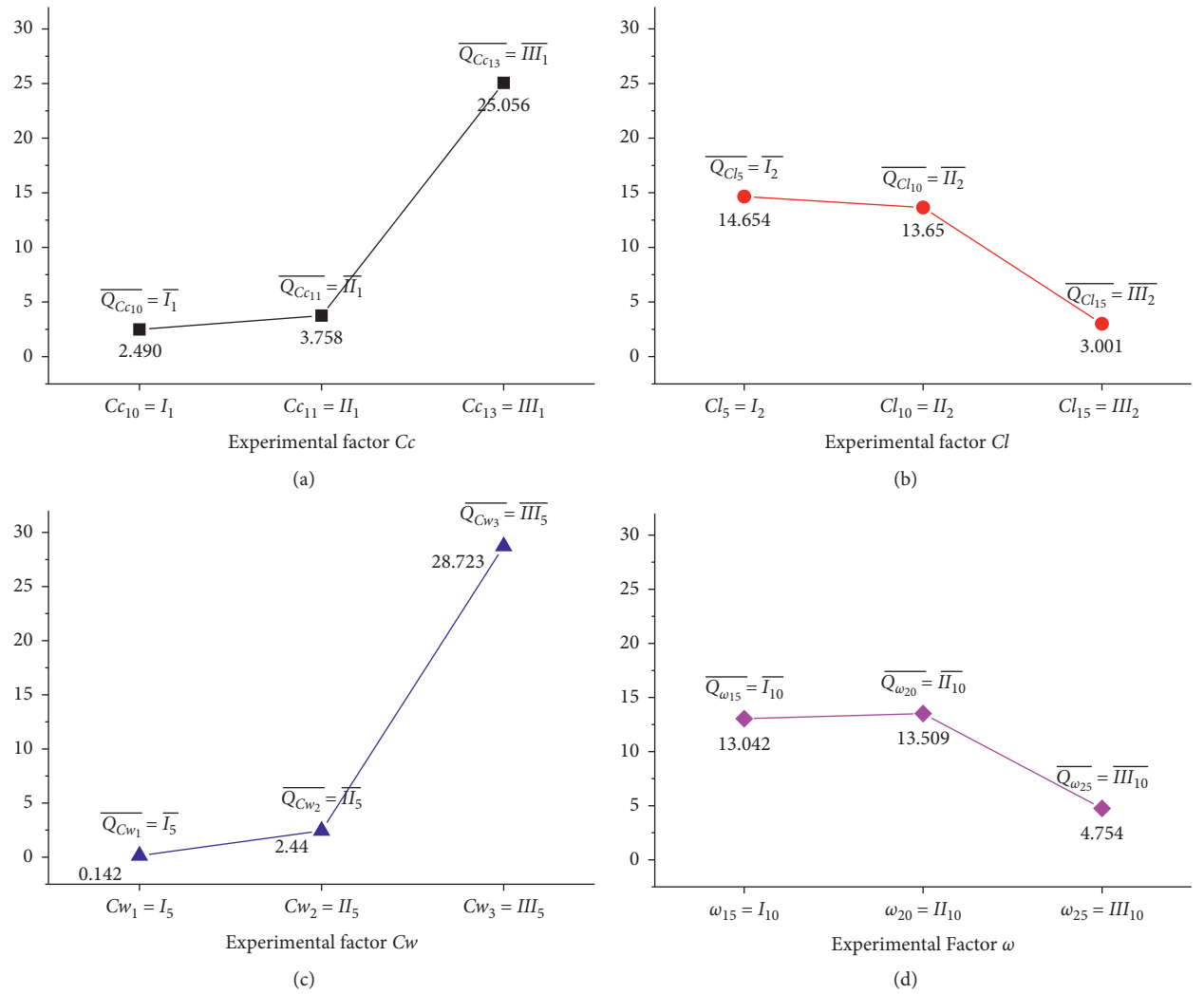

Figure 14: Relationship between the experimental factors and the rate of flow.

this experimental factor is the main factor. Namely, the difference between the average rate of flow corresponding to different levels of the experimental factors is large, which is reflected in Figure 14, and the points corresponding to the three levels of the experimental factors differ greatly in the longitudinal coordinates. In contrast, if one experimental factor has little influence on the experimental result, then this experimental factor is the secondary factor. That is, the difference between the average rate of flow corresponding to different levels of the experimental factors is small, which is reflect in Figure 14, and the points corresponding to the three levels of the experimental factors differ little in the longitudinal coordinates.

The absolute average values of the difference between $\overline{\mathrm{I}_j}$, $\overline{\mathrm{II}_j}$, and $\overline{\mathrm{III}_j}$ in Table 4 are

$$\begin{aligned}
\frac{\left|\overline{\mathrm{I}_1} - \overline{\mathrm{II}_1}\right| + \left|\overline{\mathrm{I}_1} - \overline{\mathrm{III}_1}\right| + \left|\overline{\mathrm{II}_1} - \overline{\mathrm{III}_1}\right|}{3} &= 15.044\left(10^{-6}\ \mathrm{m}^3/\mathrm{s}\right),\\
\frac{\left|\overline{\mathrm{I}_2} - \overline{\mathrm{II}_2}\right| + \left|\overline{\mathrm{I}_2} - \overline{\mathrm{III}_2}\right| + \left|\overline{\mathrm{II}_2} - \overline{\mathrm{III}_2}\right|}{3} &= 7.769\left(10^{-6}\ \mathrm{m}^3/\mathrm{s}\right),\\
\frac{\left|\overline{\mathrm{I}_5} - \overline{\mathrm{II}_5}\right| + \left|\overline{\mathrm{I}_5} - \overline{\mathrm{III}_5}\right| + \left|\overline{\mathrm{II}_5} - \overline{\mathrm{III}_5}\right|}{3} &= 19.054\left(10^{-6}\ \mathrm{m}^3/\mathrm{s}\right),\\
\frac{\left|\overline{\mathrm{I}_{10}} - \overline{\mathrm{II}_{10}}\right| + \left|\overline{\mathrm{I}_{10}} - \overline{\mathrm{III}_{10}}\right| + \left|\overline{\mathrm{II}_{10}} - \overline{\mathrm{III}_{10}}\right|}{3} &= 5.837\left(10^{-6}\ \mathrm{m}^3/\mathrm{s}\right).
\end{aligned} \tag{4}$$

The maximum absolute average value of the difference between the three levels of each experimental factor is factor

Cw, followed by factors Cc and Cl and factor ω. In addition, the influences of Cw and Cc on the experimental results are more notable than those of Cl and ω. The result indicates that the order of influence of each factor on the stability of soil layer is the crack width, particle composition, soil layer thickness, and water content and also indicates that the influence of crack width and particle composition on the failure of soil layer is greater than that of the soil layer thickness and water content.

As seen from Figure 14, the order of influence of the particle composition on the rate of flow is $Cc_{13} > Cc_{11} > Cc_{10}$, which shows that the higher the sand content in the soil is, the worse the stability of the soil layer is. The order of influence of the soil layer thickness on the rate of flow is $Cl_5 > Cl_{10} > Cl_{15}$; that is, the smaller the soil layer thickness is, the more likely it is that the soil layer will fail. The order of influence of the crack width on the rate of flow is $Cw_3 > Cw_2 > Cw_1$, which indicates that the larger the crack width is, the worse the stability of the soil layer is. The order of influence of the water content on the rate of flow is $\omega_{20} > \omega_{15} > \omega_{25}$, which indicates that the stability of the soil layer decreases first and then increases with increasing water content and that soil layer is prone to further failure when the water content is 20%.

In addition, Table 4 also shows that $Q_{Cc_{13}}$ (III_1) is significantly larger than $Q_{Cc_{10}}$ (I_1) and $Q_{Cc_{11}}$ (II_1), and Q_{Cw_3} (III_5) is significantly larger than Q_{Cw_1} (I_5) and Q_{Cw_2} (II_5), while $Q_{Cl_{15}}$ (III_2) is significantly smaller than Q_{Cl_5} (I_2) and $Q_{Cl_{10}}$ (II_2). These observations indicate that when the sand content in the soil is higher than 50% and the crack width is larger than 2.0 mm, the soil layer is prone to further failure. When the soil layer thickness is 15.0 cm, the stability of the soil layer is better than those of the 10.0 cm or 5.0 cm; that is, increasing the thickness of the soil layer can increase the ability of soil layer to resist further failure.

4.3. Variance Analysis of the Experimental Results

4.3.1. Sum of Squares of Deviations of Experimental Factors. Taking Cc as an example, the calculation method of the sum of squares of deviations of experimental factor is illustrated. Level 1 (Cc_{10}) of experimental factor Cc appeared in experiment Nos. 1–9 in Table 3, and the sum of the rate of flow of the nine groups of experimental results is

$$Q_{Cc_{10}} = Q_1 + Q_2 + Q_3 + Q_4 + Q_5 + Q_6 + Q_7 + Q_8 + Q_9, \tag{5}$$

level 2 (Cc_{11}) of experimental factor Cc appeared in experiment Nos. 10–18 in Table 3, and the sum of the rate of flow of the nine groups of experimental results is

$$Q_{Cc_{11}} = Q_{10} + Q_{11} + Q_{12} + Q_{13} + Q_{14} + Q_{15} + Q_{16} + Q_{17} + Q_{18}, \tag{6}$$

level 3 (Cc_{13}) of experimental factor Cc appeared in experiment Nos. 19–27 in Table 3, and the sum of the rate of flow of the nine groups of experimental results is

$$Q_{Cc_{13}} = Q_{19} + Q_{20} + Q_{21} + Q_{22} + Q_{23} + Q_{24} + Q_{25} + Q_{26} + Q_{27}. \tag{7}$$

The soil layer in experiment No. 21 and No. 24 is destroyed, and their experimental results are $\infty\,m^3/s$. Because the value ∞ cannot participate in the calculation, the rate of flow result in experiment No. 21 and No. 24 is calculated to be a larger value of 100 ($10^{-6}\,m^3/s$).

Hence, the sum of squares of deviations of experimental factor Cc is

$$S_{Cc} = 9\left(\frac{Q_{Cc_{10}}}{9} - \overline{Q}\right)^2 + 9\left(\frac{Q_{Cc_{11}}}{9} - \overline{Q}\right)^2 + 9\left(\frac{Q_{Cc_{13}}}{9} - \overline{Q}\right)^2, \tag{8}$$

where $\overline{Q}$ is the average rate of flow of the 27 groups of experimental results and $\overline{Q} = 1/27\sum_{i=1}^{27} Q_i$.

Expansion of formula (8) results in

$$\begin{aligned} S_{Cc} &= \frac{Q_{Cc_{10}}^2 + Q_{Cc_{11}}^2 + Q_{Cc_{13}}^2}{9} + 27\overline{Q}^2 - 2\overline{Q}\left(Q_{Cc_{10}} + Q_{Cc_{11}} + Q_{Cc_{13}}\right) \\ &= \frac{Q_{Cc_{10}}^2 + Q_{Cc_{11}}^2 + Q_{Cc_{13}}^2}{9} + \overline{Q}\cdot\sum_{i=1}^{27} Q_i - 2\overline{Q}\cdot\sum_{i=1}^{27} Q_i \\ &= \frac{Q_{Cc_{10}}^2 + Q_{Cc_{11}}^2 + Q_{Cc_{13}}^2}{9} - \frac{1}{27}\left(\sum_{i=1}^{27} Q_i\right)^2. \end{aligned} \tag{9}$$

Let $\sum_{i=1}^{27} Q_i$ be factor G and $G^2/27$ be factor CT; then, formula (9) can be simplified as follows:

$$S_{Cc} = \frac{Q_{Cc_{10}}^2 + Q_{Cc_{11}}^2 + Q_{Cc_{13}}^2}{9} - \mathrm{CT}. \tag{10}$$

The data in Table 3 are substituted into formula (10) to obtain $S_{Cc} = 2893.388$.

In the same way, the sum of squares of deviations of experimental factors Cl, Cw, and ω can be calculated as

$$\begin{aligned} S_{Cl} &= \frac{Q_{Cl_5}^2 + Q_{Cl_{10}}^2 + Q_{Cl_{15}}^2}{9} - \mathrm{CT} = 750.586, \\ S_{Cw} &= \frac{Q_{Cw_1}^2 + Q_{Cw_2}^2 + Q_{Cw_3}^2}{9} - \mathrm{CT} = 4539.002, \\ S_{\omega} &= \frac{Q_{\omega_{15}}^2 + Q_{\omega_{20}}^2 + Q_{\omega_{25}}^2}{9} - \mathrm{CT} = 436.702. \end{aligned} \tag{11}$$

The sum of squares of deviations of the above experimental factors can also be calculated on the orthogonal table, which is shown in Table 5.

As shown in Table 5, I_j represents the sum of the experimental results corresponding to level 1 of column j, and II_j represents the sum of the experimental results corresponding to level 2 of column j, while III_j represents the sum of the experimental results corresponding to level 3 of column j. Therefore, I_1 is $Q_{Cc_{10}}$, II_1 is $Q_{Cc_{11}}$, and III_1 is $Q_{Cc_{13}}$. S_j represents the sum of squares of deviations of the

Table 5: Calculating table of the sum of squares of deviations of experimental factors.

Experiment number	Column Factor	1 Cc	2 Cl	5 Cw	10 ω	13	Experimental results: Q_i (10^{-6} m^3/s)
1		1	1	1	1	1	0.000
2		1	1	2	2	2	1.517
⋮	⋮	⋮	⋮	⋮	⋮	⋮	⋮
26		3	3	2	2	2	0.975
27		3	3	3	3	3	12.167
I_j		22.409	131.882	1.274	117.374	121.333	
II_j		33.824	122.850	21.958	121.583	35.400	
III_j		225.507	27.008	258.508	42.783	125.007	
I_j^2		502.163	17392.862	1.623	13776.656	14721.697	
II_j^2		1144.063	15092.123	482.154	14782.426	1253.160	
III_j^3		50853.407	729.432	66826.386	1830.385	15626.750	
$S_j = (I_j^2 + II_j^2 + III_j^2)/9 - CT$		2893.388	750.586	4539.002	436.702	571.385	

The soil layer in experiment No. 21 and No. 24 is destroyed, and their experimental results tend to ∞ m^3/s. Because the value ∞ cannot participate in the calculation, the rate of flow result in experiment No. 21 and No. 24 is calculated to be a larger value of 100 (10^{-6} m^3/s).

experimental results in column j; hence, S_1 is S_{Cc}, S_2 is S_{Cl}, S_5 is S_{Cw}, and S_{10} is S_ω.

4.3.2. Sum of Squares of Deviations of the Interaction between the Experimental Factors. The interaction between two experimental factors accounts for two columns in the orthogonal table; therefore, the sum of squares of deviations of the interaction between two factors is the sum of the sum of squares of deviations of the two columns. Therefore, the sum of squares of deviations of $S_{\mathrm{Cc\times Cl}}$ is

$$\begin{aligned} S_{\mathrm{Cc\times Cl}} = S_3 + S_4 &= \left(\frac{\mathrm{I}_3^2 + \mathrm{II}_3^2 + \mathrm{III}_3^2}{9} - \mathrm{CT}\right) \\ &+ \left(\frac{\mathrm{I}_4^2 + \mathrm{II}_4^2 + \mathrm{III}_4^2}{9} - \mathrm{CT}\right) \\ &= 641.506 + 545.085 \\ &= 1186.591. \end{aligned} \tag{12}$$

Similarly, $S_{\mathrm{Cc\times Cw}}$, $S_{\mathrm{Cc}\times\omega}$, and $S_{\mathrm{Cl\times Cw}}$ can be obtained:

$$\begin{aligned} S_{\mathrm{Cc\times Cw}} = S_6 + S_7 &= \left(\frac{\mathrm{I}_6^2 + \mathrm{II}_6^2 + \mathrm{III}_6^2}{9} - \mathrm{CT}\right) \\ &+ \left(\frac{\mathrm{I}_7^2 + \mathrm{II}_7^2 + \mathrm{III}_7^2}{9} - \mathrm{CT}\right) \\ &= 2484.838 + 2585.032 \\ &= 5069.870, \\ S_{\mathrm{Cc}\times\omega} = S_{11} + S_{12} &= \left(\frac{\mathrm{I}_{11}^2 + \mathrm{II}_{11}^2 + \mathrm{III}_{11}^2}{9} - \mathrm{CT}\right) \\ &+ \left(\frac{\mathrm{I}_{12}^2 + \mathrm{II}_{12}^2 + \mathrm{III}_{12}^2}{9} - \mathrm{CT}\right) \\ &= 636.161 + 484.380 \\ &= 1120.541, \\ S_{\mathrm{Cl\times Cw}} = S_8 + S_9 &= \left(\frac{\mathrm{I}_8^2 + \mathrm{II}_8^2 + \mathrm{III}_8^2}{9} - \mathrm{CT}\right) \\ &+ \left(\frac{\mathrm{I}_9^2 + \mathrm{II}_9^2 + \mathrm{III}_9^2}{9} - \mathrm{CT}\right) \\ &= 588.957 + 540.045 \\ &= 1129.002. \end{aligned} \tag{13}$$

The sum of squares of deviations of the interaction between experimental factors can also be calculated on the orthogonal table, which is shown in Table 6.

4.3.3. Sum of Squares of Deviations of the Experimental Error. The sum of squares of deviations of the experimental error can be calculated by the sum of squares of deviations of the blank columns without experimental factors arranged in the orthogonal table. In this experiment, the error can be estimated by the sum of squares of deviations in column 13 of Table 3 because column 13 does not arrange the experimental factor, and the sum of squares of deviations of column 13 does not include the difference between the levels of experimental factors but only reflects the magnitude of experimental errors.

In addition, if the sum of squares of deviations of the other columns is close to the sum of squares of deviations of the blank column (column 13); then, the sum of squares of deviations of this column can be combined with the sum of squares of deviations of the blank column as an error estimate, which can make the error estimate more accurate.

According to Tables 5 and 6, the sum of squares of deviations of columns 4, 8, and 9 in this experiment is close to the sum of squares of deviations of the blank column (column 13). Therefore, S_4, S_8, and S_9 can also be classified as errors as follows:

$$S_e = S_{13} + S_4 + S_8 + S_9. \tag{14}$$

The data in Tables 5 and 6 are substituted into formula (14) to obtain $S_e = 2245.472$.

4.3.4. Saliency Detection of Experimental Factors and Their Interactions. According to formula (8) for the calculation the sum of squares of deviations, it can be seen that the sum of squares of deviations may be large if the amount of data is large. That is, the sum of squares of deviations is related not only to the change in data itself but also to the amount of data. Therefore, the influence of the amount of data on the sum of squares of deviations is eliminated by introducing the free degree in orthogonal experiment, namely, comparing the average sum of squares of deviations S_A/f_A with S_e/f_e, where f_A is the free degree of the sum of squares of deviations of experimental factor A and f_e is the free degree of the sum of squares of deviations of experimental error.

For orthogonal experiments, there are

$$\begin{aligned} f_{\mathrm{total}} &= n_{\mathrm{total}} - 1, \\ f_A &= n_A - 1, \\ f_{A\times B} &= f_A \times f_B, \end{aligned} \tag{15}$$

where n_{total} is the total number of experiments and n_A is the level amount of experimental factor A.

Therefore, for this experiment, $f_{\mathrm{total}} = 27 - 1 = 26$, $f_{\mathrm{Cc}} = 3 - 1 = 2$, $f_{\mathrm{Cl}} = 3 - 1 = 2$, $f_{\mathrm{Cw}} = 3 - 1 = 2$, $f_\omega = 3 - 1 = 2$, $f_{\mathrm{Cc\times Cl}} = 2 \times 2 = 4$, $f_{\mathrm{Cc\times Cw}} = 2 \times 2 = 4$, $f_{\mathrm{Cc}\times\omega} = 2 \times 2 = 4$, and $f_{\mathrm{Cl\times Cw}} = 2 \times 2 = 4$.

According to formula (14),

$$f_e = f_{\mathrm{total}} - f_{13} - f_4 - f_8 - f_9 = 26 - 2 - 2 - 2 - 2 = 18. \tag{16}$$

Table 6: Calculating table of the sum of squares of deviations of interaction between experimental factors.

Experiment number	Column	3	4	6	7	8	9	11	12	Experimental results: Q_i (10^{-6} m^3/s)
	Factor		Cc × Cl		Cc × Cw		Cl × Cw		Cc × ω	
1		1	1	1	1	1	1	1	1	0.000
2		1	1	2	2	2	2	2	2	1.517
⋮	⋮	⋮	⋮	⋮	⋮	⋮	⋮	⋮	⋮	⋮
26		2	1	1	3	1	3	3	2	0.975
27		2	1	2	1	2	1	1	3	12.167
I_j		124.474	36.800	39.607	218.450	117.900	37.008	32.133	126.316	
II_j		31.875	119.933	215.776	32.424	34.816	123.608	124.458	115.025	
III_j		125.391	125.007	26.357	30.866	129.024	121.124	125.149	40.399	
I_j^2		15493.777	1354.240	1568.714	47720.403	13900.410	1369.592	1032.530	15955.732	
II_j^2		1016.016	14383.924	46559.282	1051.316	1212.154	15278.938	15489.794	13230.751	
III_j^2		15722.903	15626.750	694.691	952.710	16647.193	14671.023	15662.272	1632.079	
$S_j = (I_j^2 + II_j^2 + III_j^2)/9 - CT$		641.506	545.085	2484.838	2585.032	588.957	540.045	636.161	484.380	

The soil layer in experiment No. 21 and No. 24 is destroyed, and their experimental results tend to ∞ m^3/s. Because the value ∞ cannot participate in the calculation, the rate of flow result in experiment No. 21 and No. 24 is calculated to be a larger value of 100 (10^{-6} m^3/s).

Table 7: Saliency detection of experimental factors and their interactions.

Factor	Sum of squares of deviations	Free degree	Average sum of squares of deviations	F Ratio	Saliency grade
Cc	$S_{Cc} = 2893.388$	$f_{Cc} = 2$	$S_{Cc}/f_{Cc} = 1446.694$	11.597	***Highly salient influence
Cl	$S_{Cl} = 750.586$	$f_{Cl} = 2$	$S_{Cl}/f_{Cl} = 375.293$	3.008	*Some influence
Cw	$S_{Cw} = 4539.002$	$f_{Cw} = 2$	$S_{Cw}/f_{Cw} = 2269.501$	18.193	***Highly salient influence
ω	$S_{\omega} = 436.702$	$f_{\omega} = 2$	$S_{\omega}/f_{\omega} = 218.351$	1.750	⊗Nonsalient influence
Cc × Cl	$S_{Cc\times Cl} = 1186.591$	$f_{Cc\times Cl} = 4$	$S_{Cc\times Cl}/f_{Cc\times Cl} = 296.648$	2.378	*Some influence
Cc × Cw	$S_{Cc\times Cw} = 5069.870$	$f_{Cc\times Cw} = 4$	$S_{Cc\times Cw}/f_{Cc\times Cw} = 1267.468$	10.160	***Highly salient influence
Cc × ω	$S_{Cc\times\omega} = 1120.541$	$f_{Cc\times\omega} = 4$	$S_{Cc\times\omega}/f_{Cc\times\omega} = 280.135$	2.246	⊗Nonsalient influence
Cl × Cw	$S_{Cl\times Cw} = 1129.002$	$f_{Cl\times Cw} = 4$	$S_{Cl\times Cw}/f_{Cl\times Cw} = 282.251$	2.263	⊗Nonsalient influence
e	$S_e = S_{13} + S_4 + S_8 + S_9 = 2245.472$	$f_e = 18$	$S_e/f_e = 124.748$		

The ratio of the average sum of squares of deviations of the experimental factors ($S_{\text{factor}}/f_{\text{factor}}$) to the average sum of squares of deviations of the errors (S_e/f_e) is called the F ratio, that is,

$$F = \frac{S_A/f_A}{S_e/f_e}. \tag{17}$$

The F ratio of the experimental factors and the interaction between the experimental factors is calculated in terms of formula (17) as follows

$$\begin{aligned}
F_{Cc} &= \frac{S_{Cc}/f_{Cc}}{S_e/f_e} = \frac{2893.388/2}{2245.472/18} = 11.597,\\
F_{Cl} &= \frac{S_{Cl}/f_{Cl}}{S_e/f_e} = \frac{750.586/2}{2245.472/18} = 3.008,\\
F_{Cw} &= \frac{S_{Cw}/f_{Cw}}{S_e/f_e} = \frac{4539.002/2}{2245.472/18} = 18.193,\\
F_{\omega} &= \frac{S_{\omega}/f_{\omega}}{S_e/f_e} = \frac{436.702/2}{2245.472/18} = 1.750,\\
F_{Cc\times Cl} &= \frac{S_{Cc\times Cl}/f_{Cc\times Cl}}{S_e/f_e} = \frac{1186.591/4}{2245.472/18} = 2.378,\\
F_{Cc\times Cw} &= \frac{S_{Cc\times Cw}/f_{Cc\times Cw}}{S_e/f_e} = \frac{5069.870/4}{2245.472/18} = 10.160,\\
F_{Cc\times\omega} &= \frac{S_{Cc\times\omega}/f_{Cc\times\omega}}{S_e/f_e} = \frac{1120.541/4}{2245.472/18} = 2.246,\\
F_{Cl\times Cw} &= \frac{S_{Cl\times Cw}/f_{Cl\times Cw}}{S_e/f_e} = \frac{1129.002/4}{2245.472/18} = 2.263.
\end{aligned} \tag{18}$$

Look up the F ratio table, and it shows the following: $F_{0.01}(2,18) = 6.01$, $F_{0.05}(2,18) = 3.55$, $F_{0.1}(2,18) = 2.62$, $F_{0.01}(4,18) = 4.58$, $F_{0.05}(4,18) = 2.93$, and $F_{0.1}(4,18) = 2.29$. Thus, the following conclusions can be drawn:

① $F_{Cc} > F_{0.01}(2,18)$, which indicates that the change in the experimental factor of soil particle composition Cc has a highly salient influence on the experimental results, which is recorded as ***.

② $F_{0.05}(2,18) > F_{Cl} > F_{0.1}(2,18)$, which indicates that the change in the experimental factor of soil layer thickness Cl has some influence on the experimental results, which is recorded as *.

③ $F_{Cw} > F_{0.01}(2,18)$, which indicates that the change in the experimental factor of crack width Cw has a highly salient influence on the experimental results, which is recorded as ***.

④ $F_{\omega} < F_{0.1}(2,18)$, which indicates that the change in the experimental factor of soil water content ω has a nonsalient influence on the experimental results, which is recorded as ⊗.

⑤ $F_{0.05}(4,18) > F_{Cc\times Cl} > F_{0.1}(4,18)$, which indicates that the interaction between soil particle composition Cc and soil layer thickness Cl has some influence on the experimental results, which is recorded as *.

⑥ $F_{Cc\times Cw} > F_{0.01}(4,18)$, which indicates that the interaction between soil particle composition Cc and crack width Cw has a highly salient influence on the experimental results, which is recorded as ***.

⑦ $F_{Cc\times\omega} < F_{0.1}(4,18)$, which indicates that the interaction between soil particle composition Cc and soil water content ω has a nonsalient influence on the experimental results, which is recorded as ⊗.

⑧ $F_{Cl\times Cw} < F_{0.1}(4,18)$, which indicates that the interaction between soil layer thickness Cl and crack width Cw has a nonsalient influence on the experimental results, which is recorded as ⊗.

The saliency detection of the above experimental factors and their interactions can be summarized as an analysis of variance table, as shown in Table 7.

5. Conclusions

In this work, based on the crack development-closure experiments, the following conclusions are obtained.

Firstly, soil particle composition and crack width have a highly salient influence on the stability of soil layer, and soil layer thickness has some influence on its stability, while water content has a nonsalient influence on the stability of soil layer. As the crack width and sand content increase and the soil layer thickness decreases, the stability of the soil layer decreases.

Secondly, the crack will reclose when the sand content in soil is less than 50% and the crack width is less than or equal to 1.0 mm, and the soil layer is prone to further failure when

the sand content in soil is more than 50% and the crack width is greater than or equal to 3.0 mm.

Thirdly, the interaction of experimental factors Cc and Cw has a highly salient influence on the stability of soil layer, while interaction of Cc and Cl has some influence on the stability of soil layer, and interaction of Cc and ω and interaction of Cl and Cw have nonsalient influence on the stability of soil layer.

Data Availability

The data used to support the findings of this study are included within the article.

Conflicts of Interest

The authors declare that they have no conflicts of interest.

Acknowledgments

This work was supported by the National Natural Science Foundation of China (41977238 and 51804339) and the China Postdoctoral Science Foundation (2019T120715 and 2018M640760).

References

[1] J. M. Zhang, Q. S. Li, Q. A. Nan, Z. G. Cao, and K. Zhang, "Study on the bionic coal & water co-mining and its technological system in the ecological fragile region of West China," *Journal of China Coal Society*, vol. 42, no. 1, pp. 66–72, 2017.

[2] M. S. Zhang, Y. Dong, R. J. Du, and X. F. Xiao, "The strategy and influence of coal mining on the groundwater resources at the energy and chemical base in the north of Shanxi," *Earth Science Frontiers*, vol. 17, no. 6, pp. 235–246, 2010.

[3] H. B. Bai, X. B. Mao, B. H. Yao, and J. H. Tang, "Research on simultaneous exploitation of coal and groundwater in LU'AN coalfield," *Chinese Journal of Rock Mechanics and Engineering*, vol. 28, no. 2, pp. 395–402, 2009.

[4] H. Bai, D. Ma, and Z. Chen, "Mechanical behavior of groundwater seepage in karst collapse pillars," *Engineering Geology*, vol. 164, pp. 101–106, 2013.

[5] M. G. Qian, J. L. Xu, and X. X. Miao, "Green technique in coal mining," *Journal of China University of Mining & Technology*, vol. 32, no. 4, pp. 343–347, 2003.

[6] M. G. Qian, X. X. Miao, and J. L. Xu, "Resources and environment harmonics (green) mining and its technological system," *Journal of Mining & Safety Engineering*, vol. 23, no. 1, pp. 1–5, 2006.

[7] M. G. Qian, "On sustainable coal mining in China," *Journal of China Coal Society*, vol. 35, no. 4, pp. 529–534, 2010.

[8] L. M. Fan, S. M. Wang, and X. D. Ma, "Typical example of new idea for water conservation and coal mining," *Mining Safety & Environmental Protection*, vol. 36, no. 1, pp. 61–65, 2009.

[9] L. M. Fan, "Development of coal mining method with water protection in fragile ecological region," *Journal of Liaoning Technical University (Natural Science)*, vol. 30, no. 5, pp. 667–671, 2011.

[10] L. M. Fan, X. D. Ma, and R. J. Ji, "Progress in engineering practice of water-preserved coal mining in western eco-environment frangible area," *Journal of China Coal Society*, vol. 40, no. 8, pp. 1711–1717, 2015.

[11] L. M. Fan, "Scientific connotation of water-preserved mining," *Journal of China Coal Society*, vol. 42, no. 1, pp. 27–35, 2017.

[12] X. K. Sun, G. J. Ma, and X. Q. Xu, "Analysis of influence of quaternary bottom boundary clay lithology on improving mining upper limit," *Safety in Coal Mines*, vol. 35, no. 6, pp. 31–33, 2004.

[13] Q. H. Dong and R. Cai, "Deformation simulation and affection analysis of clay layer under unconsolidated water-bearing strata during mining," *Energy Technology and Management*, no. 6, pp. 53–60, 2006.

[14] Z. P. Meng, Y. F. Gao, A. H. Lu, R. Wang, X. Qiao, and C. Y. Huang, "Water inrush risk evaluation of coal mining under quaternary alluvial water and reasonable design method of waterproof coal pillar," *Journal of Mining & Safety Engineering*, vol. 30, no. 1, pp. 23–29, 2013.

[15] F. Du, H. B. Bai, H. F. Huang, and G. H. Jiang, "Mechanical analysis of periodic weighting of main roof in longwall top coal caving face with thin bedrock roof," *Journal of China University of Mining & Technology*, vol. 42, no. 3, pp. 362–369, 2013.

[16] D. Zhang, G. Fan, L. Ma, and X. Wang, "Aquifer protection during longwall mining of shallow coal seams: a case study in the Shendong Coalfield of China," *International Journal of Coal Geology*, vol. 86, no. 2-3, pp. 190–196, 2011.

[17] W. Qiao, W. Li, T. Li, J. Chang, and Q. Wang, "Effects of coal mining on shallow water resources in semiarid regions: a case study in the shennan mining area, Shaanxi, China," *Mine Water and the Environment*, vol. 36, no. 1, pp. 104–113, 2017.

[18] D. Ma, X. X. Miao, H. B. Bai et al., "Impact of particle transfer on flow properties of crushed mudstones," *Environmental Earth Science*, vol. 75, p. 593, 2016.

[19] D. Ma, H. Duan, X. Li, Z. Li, Z. Zhou, and T. Li, "Effects of seepage-induced erosion on nonlinear hydraulic properties of broken red sandstones," *Tunnelling and Underground Space Technology*, vol. 91, Article ID 102993, 2019.

[20] Y. Xu, Y. Luo, J. Li, K. Li, and X. Cao, "Water and sand inrush during mining under thick unconsolidated layers and thin bedrock in the Zhaogu No. 1 Coal Mine, China," *Mine Water and the Environment*, vol. 37, no. 2, pp. 336–345, 2018.

[21] R. K. Tiwary, "Environmental impact of coal mining on water regime and its management," *Water, Air, and Soil Pollution*, vol. 132, no. 1-2, pp. 185–199, 2001.

[22] R. Dhakate, V. S. Singh, and G. K. Hodlur, "Impact assessment of chromite mining on groundwater through simulation modeling study in Sukinda chromite mining area, Orissa, India," *Journal of Hazardous Materials*, vol. 160, no. 2-3, pp. 535–547, 2008.

[23] O. Arkoc, S. Ucar, and C. Ozcan, "Assessment of impact of coal mining on ground and surface waters in Tozakl coal field, Kırklareli, northeast of Thrace, Turkey," *Environmental Earth Sciences*, vol. 75, no. 6, p. 514, 2016.

[24] D. Ma, H. Duan, J. Liu, X. Li, and Z. Zhou, "The role of gangue on the mitigation of mining-induced hazards and environmental pollution: an experimental investigation," *Science of the Total Environment*, vol. 664, pp. 436–448, 2019.

[25] D. Ma, J. Wang, X. Cai et al., "Effects of height/diameter ratio on failure and damage properties of granite under coupled bending and splitting deformation," *Engineering Fracture Mechanics*, vol. 220, Article ID 106640, 2019.

[26] G. M. Wu, H. B. Bai, B. Du, L. Y. Wu, S. X. He, and H. Li, "Study on the failure mechanism of clay layer overlying thin bedrock in coal seam mining," *Environmental Earth Sciences*, vol. 78, no. 10, p. 315, 2019.

[27] V. Palchik, "Formation of fractured zones in overburden due to longwall mining," *Environmental Geology*, vol. 44, no. 1, pp. 28–38, 2003.

[28] Y. C. Xu, "Engineering characteristics of deep clay and its application in coal mining under building structure, railway and water body," *Coal Science and Technology*, vol. 32, no. 11, pp. 21–23, 2004.

[29] L. Z. Zhang, Q. H. Dong, X. C. Zhang, X. T. Gao, and K. Y. Zhan, "Study on self-healing ability of mining cracks in remoulded cohesive soil in loose layer," *Energy Technology and Management*, vol. 1, pp. 57–60, 2010.

[30] W. P. Li, Q. Q. Wang, and X. Q. Li, "Reconstruction of aquifuge: the engineering geological study of N2 laterite located in key aquifuge concerning coal mining with water protecting in Northwest China," *Journal of China Coal Society*, vol. 42, no. 1, pp. 88–96, 2017.

[31] S. Kakuturu and L. N. Reddi, "Mechanistic model for self-healing of core cracks in earth dams," *Journal of Geotechnical and Geoenvironmental Engineering*, vol. 132, no. 7, pp. 890–901, 2006.

[32] D. A. Sun, L. Wang, and L. Li, "Stability of unsaturated soil slopes with cracks under steady-infiltration conditions," *International Journal of Geomechanics*, vol. 19, no. 6, Article ID 04019044, 2019.

[33] J. Zhang, J. Peng, L. Zeng, J. Li, and F. Li, "Rapid estimation of resilient modulus of subgrade soils using performance-related soil properties," *International Journal of Pavement Engineering*, pp. 1–8, 2019.

[34] S. Savage, K. Douglas, R. Fell, W. Peirson, and R. Berndt, "Modeling the erosion and swelling of the sides of transverse cracks in embankment dams," *Journal of Geotechnical and Geoenvironmental Engineering*, vol. 145, no. 5, Article ID 04019015, 2019.

[35] T. D. Vo, A. Pouya, S. Hemmati, and A. M. Tang, "Modelling desiccation crack geometry evolution in clayey soils by analytical and numerical approaches," *Canadian Geotechnical Journal*, vol. 56, no. 5, pp. 720–729, 2019.

[36] D. Ma, J. Wang, and Z. Li, "Effect of particle erosion on mining-induced water inrush hazard of karst collapse pillar," *Environmental Science and Pollution Research*, vol. 26, no. 19, pp. 19719–19728, 2019.

[37] S. Zhang and J. J. Sheng, "Effect of water imbibition on hydration induced fracture and permeability of shale cores," *Journal of Natural Gas Science and Engineering*, vol. 45, pp. 726–737, 2017.

[38] J. Lee and J. W. Hong, "Morphological aspects of crack growth in rock materials with various flaws," *International Journal for Numerical and Analytical Methods in Geomechanics*, vol. 43, no. 10, pp. 1854–1866, 2019.

[39] K. He, C. Chen, and B. Li, "Case study of a rockfall in Chongqing, China: movement characteristics of the initial failure process of a tower-shaped rock mass," *Bulletin of Engineering Geology and the Environment*, vol. 78, no. 5, pp. 3295–3303, 2019.

[40] M. Saadat and A. Taheri, "A numerical approach to investigate the effects of rock texture on the damage and crack propagation of a pre-cracked granite," *Computers and Geotechnics*, vol. 111, pp. 89–111, 2019.

[41] Q. X. Huang, B. N. Wei, and W. Z. Zhang, "Study of downward crack closing of clay aquiclude in shallowly buried coal seam," *Journal of Mining & Safety Engineering*, vol. 27, no. 1, pp. 35–39, 2010.

[42] J. H. Zhang, J. H. Peng, J. L. Zheng, and Y. S. Yao, "Characterisation of stress and moisture-dependent resilient behaviour for compacted clays in South China," *Road Materials and Pavement Design*, pp. 1–14, 2018.

[43] J. H. Zhang, J. H. Peng, J. L. Zheng, L. L. Dai, and Y. S. Yao, "Prediction of resilient modulus of compacted cohesive soils in South China," *International Journal of Geomechanics*, vol. 19, no. 7, Article ID 04019068, 2019.

[44] X. Q. Fang, H. F. Huang, T. Jin, and J. B. Bai, "Movement rules of overlying strata around longwall mining in thin bedrock with thick surface soil," *Chinese Journal of Rock Mechanics and Engineering*, vol. 27, no. 1, pp. 2700–2706, 2008.